Kinetics, selectivity and scale up of the Fischer-Tropsch synthesis

van der Laan, Gerard Pieter

7

Multicomponent Reaction Engineering Model for Fischer-Tropsch Synthesis in Commercial Scale Slurry Bubble Column Reactors

Abstract

A multicomponent mathematical model is presented for a large scale slurry bubble column reactor operating in the heterogeneous or churn-turbulent flow regime. The model accounts for both the Fischer-Tropsch reaction as well as the water gas shift reaction and the individual paraffin and olefin formation rates. It provides all the data necessary for reliable scale up, process optimization, and prediction of the performance of industrial scale Fischer-Tropsch bubble column reactors.

7.1 Introduction

Synthesis gas (CO and H_2) from coal or natural gas can be converted in the Fischer-Tropsch (FT) process to a multicomponent mixture of predominantly linear hydrocarbons. The FT synthesis in slurry bubble column reactors (SBCR) is very attractive relative to fixed bed reactors [1]. The advantages are: 1) Low pressure drop over the reactor. 2) Excellent heat transfer characteristics resulting in stable reactor temperatures. 3) No diffusion limitations. 4) Possibility of continuous refreshment of catalyst particles. 5) Relatively simple construction and low investment costs. Mathematical modeling of a FT SBCR was reviewed by Saxena et al. [1] and more recently by Saxena [2]. The bottleneck appears to be the lack of reliable kinetic equations for all products and reactants based on realistic reaction mechanisms.

A summary of previous slurry bubble column reactor models for the Fischer-Tropsch synthesis is given in Table 7.1. Most models are only applicable in small scale slurry bubble columns operating in the homogeneous regime. However, the churn-turbulent or heterogeneous regime is the most optimal one for the FT synthesis [13]. In this regime, there is a range of bubble sizes. The gas bubbles can be divided into two classes: 1) the small bubbles with a constant bubble diameter less than 0.01 m, and 2) the large bubbles: bubbles larger than 0.01 m with irregular shape and varying size. The mixing behavior of both classes is completely different due to the difference in rise velocity. Krishna and co-workers modeled a slurry bubble column containing cobalt catalyst particles with the use of flow patterns for the large and small bubbles [13, 16, 17].

Appropriate rate equations for both the Fischer-Tropsch and the water gas shift reaction are needed for modeling of bubble columns operated with iron catalysts. Kuo [9], Stenger and Satterfield [10], Prakash and Bendale [11], Prakash [12], and Inga and Morsi [15] included rate expressions for the FT and WGS reactions to obtain accurate hydrogen and carbon monoxide axial concentration profiles. Until now, none of the available literature models can describe the complete product distribution of the FT synthesis at industrial conditions (high temperature and pressure) as a function of overall consumption of synthesis gas components and operating conditions.

This study will investigate an iron-based Fischer-Tropsch SBCR operating in the heterogeneous flow regime. The model takes into account both the water gas shift and the FT reactions, as well as individual hydrocarbon product formation rates. Here, multicomponent vapor-liquid equilibria (VLE) with detailed kinetic expressions for all reactants and hydrocarbon products are combined with SBCR hydrodynamics and

Table 7.1 Comparison of reaction engineering models for the Fischer-Tropsch synthesis in slurry bubble column reactors.

Reference	Gas phase	Liquid phase	Catalyst distribution	Energy balance	Components	FT Table 7.2	WGS
Calderbank et al. [3]	PF	PF	uniform	isothermal	H_2	1	-
Satterfield and Huff [4]	PF	PM	uniform	isothermal	H_2	1	-
Deckwer et al. [5]	PF	PM	uniform	isothermal	H_2	1	-
Deckwer et al. [6]	AD	AD	non-uniform	non-isothermal	H_2	1	-
Bukur [7]	PF	PF, PM	uniform	isothermal	H_2	1	
Stern et al. [8]	PF	PM	uniform	isothermal	H_2, CO, CO_2, H_2O, CH_4, C_5H_{10}	1	-
Kuo [9]	PF	PM, PF, AD	non-uniform	isothermal	H_2	1	-
Kuo [9]	PF	PF	non-uniform	isothermal	H_2, CO, CO_2, H_2O	2	2
Stenger and Satterfield [10]	AD	AD	non-uniform	isothermal	H_2,CO,CO_2,H_2O, C_5H_{10}	1	1
Prakash and Bendale [11]	AD	AD	non-uniform	isothermal	H_2,CO,CO_2,H_2O, C_{1-3}	2	2
Prakash [12]	AD	AD	non-uniform	isothermal	H_2,CO,CO_2,H_2O, C_{1-3}	2	2
De Swart [13][1]	AD	AD	non-uniform	non-isothermal	H_2	1	-
De Swart [13][2]	PF	PM	uniform	isothermal	H_2	1	-
Mills et al. [14]	AD	AD	non-uniform	non-isothermal	H_2	1	-
Inga and Morsi [15]	PF	MC	uniform	isothermal	H_2, CO, H_2O	1, 3	2
Krishna and Maretto [16][2]	PF	PM	uniform	isothermal	H_2, CO	3	-
Our model[2]	PF	PM	uniform	isothermal	H_2,CO,CO_2,H_2O,N_2, C_{1-100}		

PF: plug flow, PM: perfectly mixed, MC: mixing cells, AD: axial dispersion

[1] Heterogeneous flow regime: Large bubbles: PF, Small bubbles and liquid: AD

[2] Heterogeneous flow regime: Large bubbles: PF, Small bubbles and liquid: PM

mass transfer characteristics to predict the detailed product composition of both gas and liquid phase as a function of operating conditions.

Table 7.2 Kinetic models for Table 7.1.

	FT kinetic expressions		WGS kinetic expressions
1	$kC_{H_2,L}$	1	$k\left(C_{CO,L}C_{H_2O,L} - C_{CO_2,L}C_{H_2,L}/K_P\right)$
2	$\dfrac{kC_{H_2,L}C_{CO,L}}{C_{CO,L} + aC_{H_2O}}$	2	$\dfrac{k\left(C_{CO,L}C_{H_2O,L} - C_{CO_2,L}C_{H_2,L}/K_P\right)}{P_{CO} + aP_{H_2O}}$
3	$\dfrac{kC_{H_2,L}C_{CO,L}}{(1 + aC_{CO,L})^2}$		

7.2 Kinetics and Hydrocarbon Selectivity

The rate expression for the FT reaction on a precipitated iron catalyst in the slurry phase proposed in Chapter 6 was used (Table 7.3):

$$R_{FT} = \frac{kP_{CO}P_{H_2}^{1/2}}{\left(1 + aP_{CO} + bP_{CO_2}\right)^2} \tag{7.1}$$

The water gas shift reaction is an exothermic and reversible reaction proceeding simultaneously with the Fischer-Tropsch reaction. Due to the WGS reaction, synthesis gas with a H_2/CO ratio below 2 can be used because excess of carbon monoxide is converted with water to carbon dioxide and hydrogen. The equilibrium constant K_P was obtained from Graaf et al. [18] and the following rate expression was used for the kinetics of the WGS (see Table 7.3 and Chapter 6):

$$R_{WGS} = \frac{k_{WGS}\left(P_{CO}P_{H_2O} - P_{CO_2}P_{H_2}/K_P\right)}{\left(P_{CO} + KP_{H_2O}\right)^2} \tag{7.2}$$

The product selectivity to α-olefins and paraffins was calculated using a recently developed selectivity model for iron catalysts, called α-Olefin Readsorption Product Distribution Model (ORPDM) (see Chapters 4 and 6). This model allows for a chain-length dependent chain growth factor due to readsorption of α-olefins. The appropriate model parameters are shown in Table 7.3 as a function of process variables (P_{CO}, P_{H_2}, $\Phi_{v,0}/W$) at a constant temperature of 523 K.

Table 7.3 Kinetic and selectivity model parameters at 523 K (Chapter 6).

Parameter	Value	Parameter	Value
t_P^1	6.5	k (mol kg^{-1} s^{-1} MPa$^{-1.5}$)	0.0339
t_P^2	1.7	a (MPa^{-1})	1.185
c	0.35	b (MPa^{-1})	0.656
k_R^2	$17.6\, k_R e^{2\,c}$	k_{WGS} (mol kg^{-1} s^{-1})	0.0292
p	$14.0 P_{H_2}^{-0.26} P_{CO}^{0.40}$	K (-)	3.07
t_O	$3.71 P_{H_2}^{-0.5}$	K_P	85.81
k_R	$8.00\ 10^{-5} \dfrac{P_{H_2}^{1.2} P_{CO}^{-0.47}}{\Phi_{v,0}/W}$		

Pressures in MPa, space velocity $\Phi_{v,0}/W$ in Nm^3 kg$_{cat}^{-1}$ s^{-1}

7.3 Model Equations

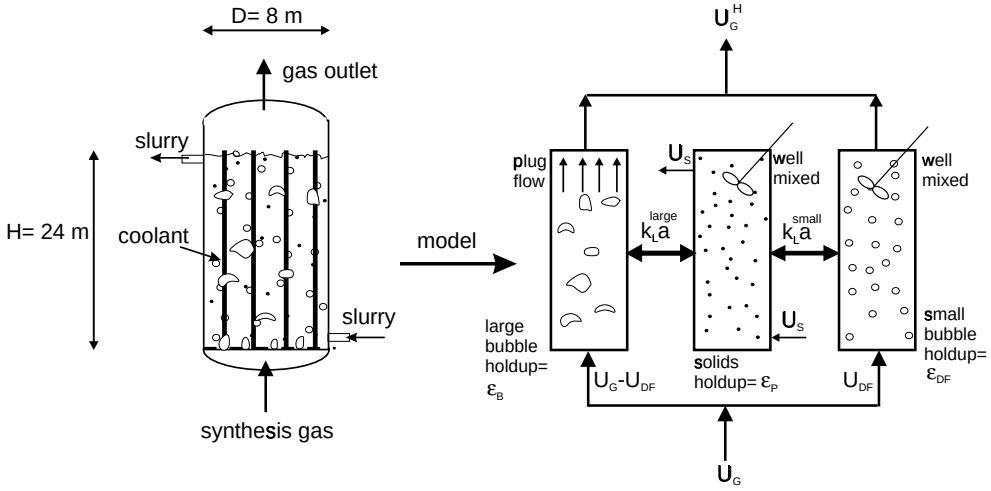

Figure 7.1 Hydrodynamic model of slurry bubble column reactor in the heterogeneous flow regime.

A mathematical description for the simulation of an industrial Fischer-Tropsch SBCR is presented. The reactor model can be applied in the heterogeneous or churn-turbulent regime (see Figure 7.1). The large bubbles are assumed to be in plug flow with a superficial gas velocity of $U_G - U_{DF}$. The superficial velocity of the gas present in the well mixed small bubbles is U_{DF}, which is equal to the total superficial gas ve-

locity at regime transition. The mathematical model for the Fischer-Tropsch synthesis is based on the following assumptions: 1) Gas-liquid mass transfer resistance is located in the liquid phase. 2) Large gas bubbles are in plug flow due to high rise velocities, typically 1-2 m s^{-1}. 3) The gas phase in the small gas bubbles, and the liquid phase are each completely mixed, due to the large reactor diameter of 8 m [6]. Catalyst distribution is uniform due to upflow of the slurry phase, the large reactor diameter and the turbulence created by the fast-rising large bubbles. 4) Hydrocarbon products, paraffins and olefins only, in the gas and liquid phase of the reactor outlet are assumed to be in equilibrium at the reactor outlet. 5) The reactor operates isothermally due to the completely mixed liquid phase. 6) The slurry velocity is constant. 7) The reactor operates at steady state conditions. 8) The effectiveness factor of the catalyst particles is equal to unity and mass and heat transfer resistances between catalyst and liquid are negligible due to the small particle size applied (50 μm).

The gas phase mass balance for component i in the *large* bubbles, rising in plug flow is:

$$\frac{d\left(U_G - U_{DF}\right) C_{i,G}^{large}}{dh} + \left(k_L a\right)_i^{large} \left(\frac{C_{i,G}^{large}}{m_i^{GL}} - C_{i,L} \right) = 0 \tag{7.3}$$

with concentrations in mol m^{-3} subject to the boundary conditions at the reactor entrance: h=0: $C_{i,G}^{large} = C_{i,G}^{in}$. The gas phase mass balance for component i in the *small* bubbles (completely mixed) is:

$$\frac{U_{DF}}{H} \left(C_{i,G}^{in} - C_{i,G}^{small} \right) = \left(k_L a\right)_i^{small} \left(\frac{C_{i,G}^{small}}{m_i^{GL}} - C_{i,L} \right) \tag{7.4}$$

The mass balance for component i in the completely mixed liquid phase can be written as:

$$1/H \int_0^H \left(k_L a\right)_i^{large} \left(\frac{C_{i,G}^{large}}{m_i^{GL}} - C_{i,L} \right) dh + \left(k_L a\right)_i^{small} \left(\frac{C_{i,G}^{small}}{m_i^{GL}} - C_{i,L} \right) + \\ + \varepsilon_L \varepsilon_P \rho_P \sum_{j=1}^{n} \nu_{ij} R_j - \frac{U_S}{H} C_{i,L} = 0 \tag{7.5}$$

where ε_L is the liquid holdup (m_L^3 m_R^{-3}), ε_P is the solids holdup (m_P^3 m_L^{-3}), ρ_P is the catalyst density, R_j is the FT (j=1) or WGS (j=2) reaction rate (mol kg_{cat}^{-1} s^{-1}), ν_{ij} is the stoichiometric coefficient for component i in the j-th reaction. The reaction heat

is removed with vertical cooling tubes of 1.5 inch diameter at a constant steam temperature T_c of 495 K. The overall heat transfer coefficient α_{eff} from slurry to coolant is estimated from the correlation of Deckwer et al. [19]:

$$\alpha_{eff} = 0.1 U_G^{0.25} \rho_S^{0.75} C_{p,S}^{0.5} g^{0.25} \eta_S^{-0.25} \lambda_S^{0.5} \tag{7.6}$$

At gas velocities higher than 0.10 m s^{-1} the heat transfer coefficient does not increase any more and is calculated from eq 7.6 with U_G equal to 0.10 m s^{-1}.

The energy balance for the slurry phase reads, assuming the catalyst and the liquid temperature to be equal:

$$\varepsilon_L \varepsilon_P \rho_P \sum_{j=1}^{n} \left(-\Delta H_{R,j}\right) R_j - \alpha_{eff} a_c (T - T_c) + \\ + \frac{U_S}{H} \left(\left(\rho_S C_{p,S} T\right)_{in} - \left(\rho_S C_{p,S} T\right)_{out} \right) = 0 \tag{7.7}$$

where a_c is the specific heat transfer area (m^{-1}), $C_{p,S}$ is the heat capacity of the slurry phase, ρ_S is the slurry density and $-\Delta H_{R,j}$ is the reaction heat of reaction j (J mol^{-1}).

The molar flow rate of the gas phase will change due to reaction. The superficial velocity is assumed to be a linear function of the overall synthesis gas conversion, X_{CO+H_2} [14]:

$$U_G = (1 + \alpha_c X_{CO+H_2}) U_G^{in} = \left(1 + \alpha_c (1+U)/(1+F) X_{H_2}\right) U_G^{in}, \tag{7.8}$$

where α_c is the contraction factor, defined as:

$$\alpha_c = \frac{U_G(X_{CO+H_2} = 1) - U_G(X_{CO+H_2} = 0)}{U_G(X_{CO+H_2} = 0)} \tag{7.9}$$

U is the usage ratio of hydrogen to carbon monoxide (-R_{H_2}/-R_{CO}) and F is the feed ratio of H_2 to CO. The reported values of α are between -0.5 and -0.65 [6]. The contraction factor α_c is determined by the product selectivity (m and n).

7.4 Hydrodynamic Parameters

The most important hydrodynamic parameters are the gas holdup of the large and small bubbles in presence of solids under Fischer-Tropsch reaction conditions. The rise velocity of the small bubbles will increase with increasing solids holdup due to enhanced coalescence according to:

$$V_{small} = V_{small}^{ref} \left(1 + 0.8 \varepsilon_P / V_{small}^{ref}\right) \tag{7.10}$$

with V_{small}^{ref} = 0.095 m s^{-1} [20]. The gas holdup at the transition from homogeneous to churn turbulent regime in the presence of a high solids loading follows from Krishna et al. [20]:

$$\varepsilon_{DF} = \varepsilon_{DF}^{ref} \left(\rho_G / \rho_G^{ref} \right)^{0.48} \left(1 - 0.7 \varepsilon_P / \varepsilon_{DF}^{ref} \right) \tag{7.11}$$

where the small bubble holdup in solids-free liquid is ε_{DF}^{ref}= 0.27 and the atmospheric density is ρ_G^{ref}= 1.3 kg m^{-3}. The corresponding superficial gas velocity at regime transition is calculated from $U_{DF} = V_{small} \varepsilon_{DF}$. The model of Krishna and Ellenberger [21] is used to predict the gas holdup of the *large* bubbles. This model is corrected for the influence of gas density according to a recent study of Letzel et al. [22]. For large bubble columns ($D > 1$ m) and high slurry concentrations ($\varepsilon_P > 0.16$), the large bubble holdup can be estimated from a combination of the correlations given by Letzel et al. [22] and Krishna et al. [20]:

$$\varepsilon_B = 0.3 \left(U_G - U_{DF} \right)^{0.58} \left(\rho_G / \rho_G^{ref} \right)^{0.5} \tag{7.12}$$

The total gas holdup in the heterogeneous regime is calculated from:

$$\varepsilon_G = \varepsilon_B + \varepsilon_{DF} \left(1 - \varepsilon_B \right) \tag{7.13}$$

The volumetric mass transfer coefficient of *large* bubbles is obtained from the relation proposed by Vermeer and Krishna [23] and more recently by Letzel et al. [22]:

$$k_L a_{ref}^{large} / \varepsilon_B = 0.5 \tag{7.14}$$

which is corrected for the mass transfer coefficient of component i by the factor:

$$k_{L,i}^{large} / k_{L,ref}^{large} = \left(D_i / D_{ref} \right)^{0.5} \tag{7.15}$$

where D_{ref}= 2 10^{-9} m^2 s^{-1}. In the same way, the volumetric mass transfer coefficient for component i of the small bubbles is defined as [16]:

$$k_L a_{ref}^{small} / \varepsilon_{DF} = 1.0 \tag{7.16}$$

7.5 Physical Properties and Flash Calculations

For calculating the physical properties of the liquid, it was assumed that the FT wax consisted of n-paraffins with a carbon number of 28 ($C_{28}H_{58}$). The physical properties at 523 K were estimated with the asymptotical behavior correlations developed by

Table 7.4 Operation conditions and physical properties.

Reactor configuration		
reactor diameter	D= 8	m
reactor height	H=30 (20% disengagement zone)	m
dispersion height	H=24	m
Operating conditions		
pressure	P= 30 10^5	Pa
temperature	T= 523	K
catalyst concentration	ε_P=0.20 - 0.35	$m_P^3\ m_L^{-3}$
superficial gas velocity	U_G= 0.15-0.40	m s^{-1}
superficial slurry velocity	U_s= 0.01	m s^{-1}
cooling tube diameter	d_c = 0.0381	m
coolant temperature	T_c= 495	K
feed composition	F= 0.5 - 2.0, y_{CO_2}=0.05, y_{inert}=0.05	-
Liquid phase (L)		
liquid viscosity	η_L= 5.95 10^{-4}	Pa s
liquid density	ρ_L= 656.7	kg m^{-3}
surface tension	σ= 0.017	N m^{-1}
liquid heat capacity	$C_{p,L}$= 2721	J kg^{-1} K^{-1}
liquid heat conductivity	λ_L = 0.181	W m^{-1} K^{-1}
Catalyst phase (P)		
catalyst diameter	d_P = 50 10^{-6}	m
catalyst density	ρ_P=1957 (Lox et al. [24])	kg m^{-3}
catalyst heat capacity	$C_{p,P}$= 993	J kg^{-1} K^{-1}
catalyst heat conductivity	λ_P= 1.7	W m^{-1} K^{-1}
Slurry phase (S)		
catalyst weight fraction	$w_P = \frac{\varepsilon_P \rho_P}{\varepsilon_P\,(\rho_P - \rho_L) + \rho_L}$ [6]	-
slurry density	$\rho_S = \varepsilon_P \rho_P + (1-\varepsilon_P)\rho_L$ [6]	kg m^{-3}
slurry viscosity	$\eta_S = \eta_L(1 + 4.5\varepsilon_P)$ [19]	Pa s
slurry heat capacity	$C_{p,S} = w_P C_{p,P} + (1-w_P)C_{p,L}$ [6]	J $kg^{-1}K^{-1}$
slurry heat conductivity	$\lambda_S = \lambda_L \frac{2\lambda_L + \lambda_P - 2\varepsilon_P(\lambda_L - \lambda_P)}{2\lambda_L + \lambda_P + \varepsilon_P(\lambda_L - \lambda_P)}$ [25]	W m^{-1} K^{-1}

Marano and Holder [26, 27] (see Table 7.4). Henry constants for CO, CO_2, H_2, H_2O, N_2 and light hydrocarbons (C_1- C_3) were obtained from Marano and Holder [28]. Diffusivities at high temperatures and pressures, necessary for calculating mass transfer coefficients, were estimated using correlations of Erkey et al. [29] based on the rough hard sphere theory. The multicomponent VLE model of Marano and Holder [28] was applied. However, we assumed ideal gas behavior of the gas phase because under the reaction conditions applied, the fugacity coefficients (upto C_{30}) as calculated with the Peng-Robinson equation of state are between 0.95 and 1.01. The equilibrium constants between vapor and liquid for non-hydrocarbons and C_{1-3} hydrocarbons were calculated from:

$$K_i \equiv y_i/x_i = H_i^{\infty}\Phi_i/P \tag{7.17}$$

where K_i is the K-value for component i, H_i^{∞} is the Henry constant for component i at infinite dilution, and Φ_i is the Poynting-factor. For the other hydrocarbons, the K-value is given by:

$$K_i = \gamma_i^{\infty} P_{i,sat}\Phi_i/P \tag{7.18}$$

where γ_i^{∞} is an activity coefficient, and $P_{i,sat}$ is the vapor pressure of pure component i. The appropriate parameter values were obtained from Marano and Holder [28]. A flash calculation using these K-values gives the final composition of the liquid and gas phase outlet of the SBCR:

$$\rho_p\overline{\varepsilon_L}\varepsilon_P V_R R_{FT}\frac{m_i}{\sum_i n\, m_i} = U_G^H A y_i C_G + U_S A x_i C_L \tag{7.19}$$

where m_i is the molar selectivity to product i with carbon number n, and C_G and C_L are the total gas and liquid concentration, respectively.

7.6 Results and Discussion

A commercial scale SBCR with diameter D= 8 m, dispersion height H= 24 m, pressure P= 3.0 MPa and temperature T= 523 K is used in our simulations. The superficial slurry velocity U_S is 0.01 m s^{-1}. The slurry enters the reactor with an inlet temperature of 423 K. The properties of the catalyst applied (Ruhrchemie LP 33/81 Fe/Cu/K on SiO_2) are: catalyst particle diameter 50 10^{-6} m, catalyst density ρ_P= 1957 kg m^{-3}. The properties of the slurry were determined using the relations of Deckwer et

Table 7.5 Physical properties and concentrations of the components in the SBCR mentioned in Figure 7.2. Operating conditions: F=1, U_G^{in}= 0.20 m s^{-1}, ε_P=0.25, D=8 m, H=24 m, T=523 K.

Component	m_i^{GL}	D_i	$C_{i,G}^{in}$	$C_{i,G,out}^{large}$	$C_{i,G}^{small}$	$C_{i,L}$
	(C_G/C_L)	(10^{-8} m^2 s^{-1})	(mol m^{-3})			
H_2	5.83	3.85	310.5	152.6	155.1	26.2
CO	4.86	1.53	310.5	125.2	129.2	25.8
CO_2	2.32	1.26	34.5	150.3	149.0	64.9
H_2O	0.85	1.89	0	53.5	53.3	62.9
N_2	5.65	1.54	34.5	44.5	44.3	7.9

al. [6, 19] (see Table 7.4). The complete reactor model consists of a system of ordinary differential equations and algebraic equations, with the corresponding boundary conditions. The set of equations was solved numerically using a backward differentiation scheme with 60 grid points using the gPROMS software package (Version 1.6a, Process Systems Enterprise, London).

The concentration gradients of CO, H_2, CO_2, H_2O and N_2 are large in the bottom of the slurry reactor. Particularly at the top of the reactor, the liquid phase is in equilibrium with the gas phase ($C_{i,L} = C_{i,G}^{large}/m_i^{GL}$, see Table 7.5). Resulting from the difference in solubility, the H_2/CO ratio in the liquid phase is larger than that in the gas feed. The liquid phase concentrations of H_2 and CO influence the chain length and olefin content of the products formed. The axial concentration profiles of CO, H_2, CO_2, H_2O and N_2 in the large gas bubbles are plotted in Figure 7.2.

Figure 7.3 shows the corresponding productivity of each individual paraffin and olefin, both in the gas and liquid phase. The model predicts the FT product distribution between the vapor and liquid phases. The lighter products with a high olefin yield are in the gas phase, and the heavier products, mainly paraffins, leave the reactor in the liquid or wax phase. Our model predicts the effect of the process conditions on the selectivity and composition of the individual phases.

The major results of our simulations on the reactor performance are shown in Figure 7.4a-b for a range of catalyst concentrations ε_P between 0.2 and 0.35, feed ratios of H_2 to CO (F) in the synthesis gas between 0.67 and 2, with a constant mole fraction of CO_2 and N_2 in the feed of 0.05 and superficial inlet gas velocity U_G^{in} from 0.15 to 0.4 m s^{-1} (see Table 7.4). Increase of the inlet gas velocity causes a decrease of the synthesis gas conversion, as expected. At low gas velocities, $U_G^{in} < 0.15$ m s^{-1},

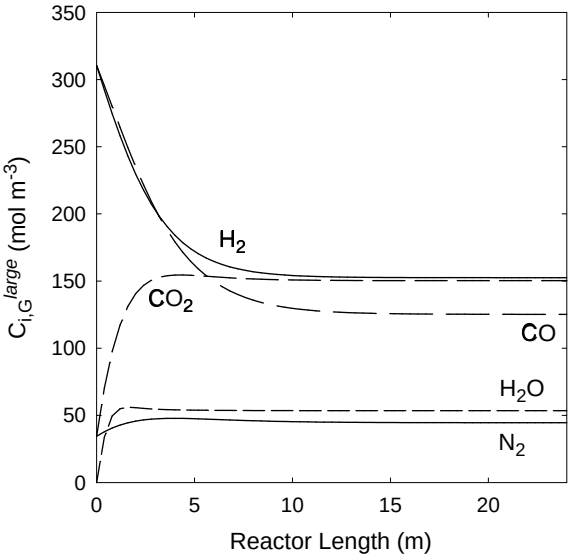

Figure 7.2 Axial concentration profiles for CO, H_2, CO_2, H_2O and N_2. Operating conditions: F=1, U_G^{in}= 0.20 m s^{-1}, ε_P=0.25, D=8 m, H=24 m, T=523 K. See also Table 7.5.

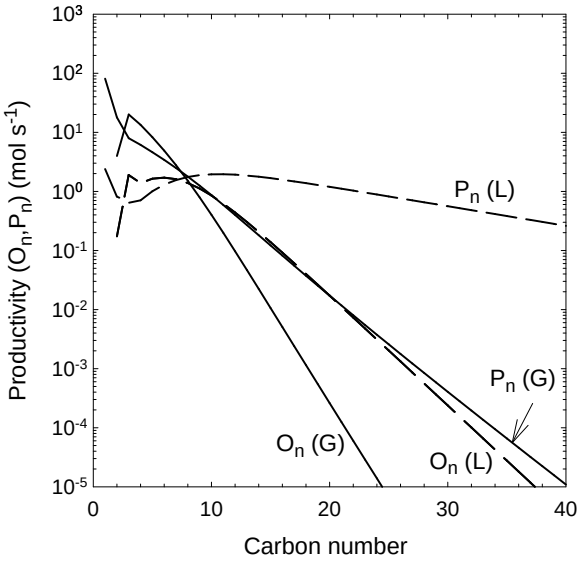

Figure 7.3 Paraffin (P_n) and olefin (O_n) production rates in the gas and liquid outlet streams (p=12.6, t_O=4.6, k_R=0.27). Operating conditions: F=1, U_G^{in}= 0.20 m s^{-1}, ε_P=0.25, D=8 m, H=24 m, T=523 K.

the synthesis gas conversion reaches a constant level of about 80 % as a consequence of the kinetic expressions with product (CO_2) inhibition. Higher conversions can be obtained when the operating conditions (P, T) or catalyst are changed or when the dispersion height is increased to, for example, H= 30 m. The reactor productivity, expressed as total hydrocarbon production in kg h^{-1} m_R^{-3}, shows an increase with increasing gas velocity. The effect of catalyst concentration on the reactor performance at F =1 is shown in Figure 7.4a. Increasing the catalyst concentration (ε_P) shows an

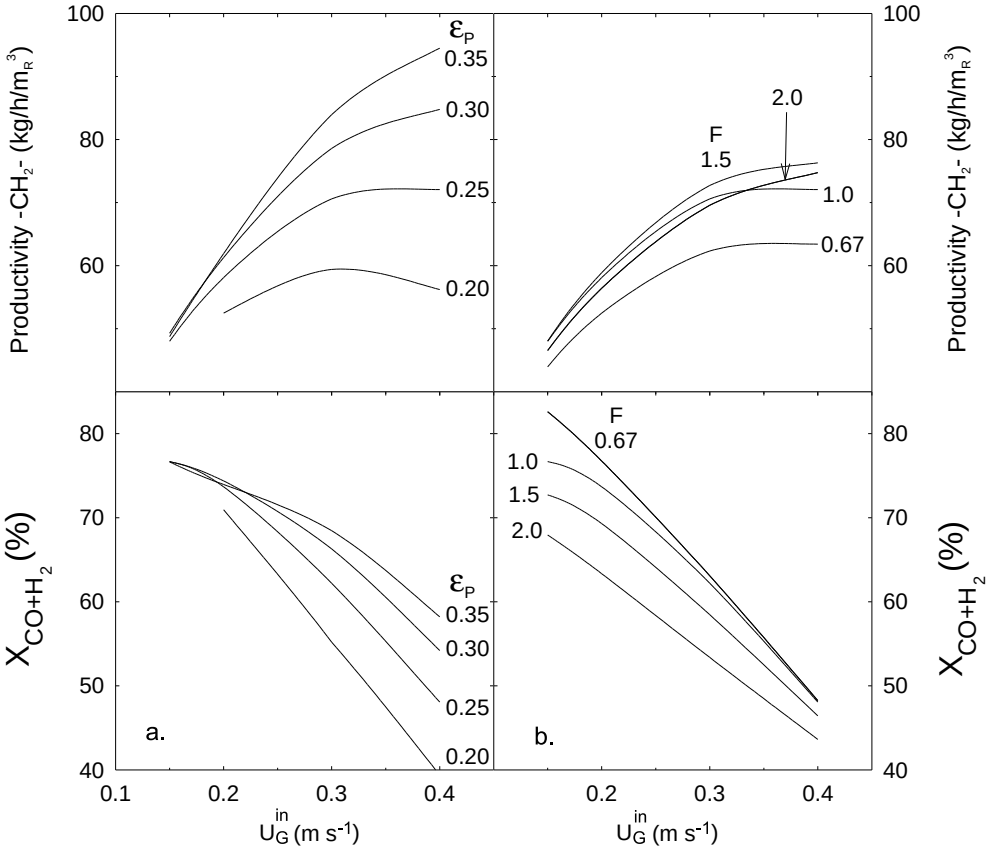

Figure 7.4 a. Effect of catalyst concentration and gas velocity on the synthesis gas conversion and productivity (F=1, T= 523 K). b. Effect of the H_2/CO feed ratio F and gas velocity on the same (ε_P=0.25, T= 523 K).

increase of the conversion and productivity. The catalyst concentration influences the concentration levels as well as ε_{DF} according to eq 7.11. The highest productivity is obtained at high catalyst concentrations (ε_P=0.35) and gas velocities up to 0.4 m s^{-1}. The effect of the feed ratio F at a constant catalyst concentration of ε_P=0.25 is given in Figure 7.4b. The decrease of the synthesis gas conversion with increasing F is mainly caused by the kinetics. At low feed ratios, conversions of CO are large due to the high water gas shift reaction rate. The optimal productivity is obtained at a feed ratio of F=1.5. The feed ratio influences the gas holdup due to changing gas density. Significantly lower gas holdup values were observed with increasing F. The number of cooling tubes required strongly depends on the productivity and varies between 600 and 1700 cooling tubes. The corresponding pitch distance varies from 0.33 to 0.20 m, which is large enough not to influence the hydrodynamics of the SBCR [16].

The effect of the feed ratio on the selectivity to several product classes is shown in Table 7.6. The total hydrocarbon (paraffin and olefin) selectivities in mass percentages were lumped in four groups: methane (w_1), light gases C_{2-4} (w_{2-4}), gasoline C_{5-10} (w_{5-10}), and a diesel/wax fraction C_{10-100} (w_{10+}). The olefin content is shown for the C_2 products ($w_{O,2}$), C_{3-4} products ($w_{O,3-4}$) and the total olefin yield of all products (w_O). The selectivities in Table 7.6 were calculated with the model parameters in Table 7.3. Increasing F has a pronounced effect on the increasing selectivity to methane and a decreasing olefin content of the product spectrum. The hydrogen concentration in the liquid bulk increases, which causes an increase of the termination to paraffins relative to olefins and a decrease of the chain growth parameter.

Table 7.6 Selectivity parameters and product selectivities (wt%) as a function of the H_2/CO feed ratio F (U_G^{in} = 0.20 m s^{-1}, ε_P = 0.25, T = 523 K).

				Product selectivity (wt%)						
F	p	t_O	k_R	w_1	w_{2-4}	w_{5-10}	w_{10+}	$w_{O,2}$	$w_{O,3-4}$	w_O
0.67	17.4	5.6	0.17	3.7	17.5	26.5	52.3	43.0	85.3	37.7
1.0	12.6	4.6	0.27	5.7	18.9	27.2	48.2	28.5	79.3	33.5
1.5	9.6	3.9	0.41	8.2	20.5	28.4	43.0	19.0	72.7	29.6
2.0	7.9	3.6	0.56	10.6	21.8	29.3	38.3	13.9	66.8	26.5

7.7 Conclusions

A mathematical design model for a large scale Fischer-Tropsch SBCR is developed. The model takes into account the water gas shift and Fischer-Tropsch reactions as well as individual hydrocarbon product formation rates. Under the operating conditions investigated the FT SBCR is mainly reaction controlled. This is caused by the limited activity of Fe catalysts on the one hand and the large value of the volumetric mass transfer coefficient of the large bubbles due to frequent bubble coalescence and breakup on the other hand. The model predicts the composition of the gaseous and liquid streams of a large scale bubble column operating in the churn-turbulent regime as a function of the operating parameters. It provides all the data necessary for reliable scale up, process optimization and prediction of the performance of industrial scale FT bubble column reactors.

List of Symbols

A	reactor area, m^2
a_c	specific cooling area, m^{-1}
C	concentration, mol m^{-3}
C_p	heat capacity, J kg^{-1} K^{-1}
D	reactor diameter, m
D	diffusion coefficient, m^2 s^{-1}
F	H_2/CO feed ratio
g	gravity acceleration factor, 9.81 m s^{-2}
h	axial position, m
H	dispersion height, m
H_i^{∞}	Henry constant, Pa
K_i	equilibrium constant (y_i/x_i)
$k_L a$	volumetric mass transfer coefficient, s^{-1}
m_i^{GL}	solubility coefficient C_G/C_L
m_i	molar selectivity
n	carbon number
P	pressure, Pa
P_i^{sat}	vapor pressure, Pa
R	gas constant, 8.314 J mol^{-1} K^{-1}
R_j	reaction rate, mol kg_{cat}^{-1} s^{-1}

T	temperature, K
U	H_2/CO consumption ratio (-R_{H_2}/-R_{CO})
U	superficial velocity, m s^{-1}
V_R	reactor volume, m^3
V_{small}	rise velocity small bubbles, m s^{-1}
w_i	weight fraction of product *i*
X_{CO+H_2}	synthesis gas conversion
X_{H_2}	hydrogen conversion
x_i	mole fraction in liquid phase
y_i	mole fraction in gas phase

Greek Letters

α_{eff}	effective heat transfer coefficient, W m^{-2} K^{-1}
α_c	contraction factor
γ_i^{∞}	liquid phase activity coefficient
$\Delta H_{R,j}$	reaction enthaphy, J mol^{-1}
ε	holdup
η_L	liquid viscosity, Pa s
λ	heat conductivity, W m^{-1} K^{-1}
ν_{ij}	stoichiometric coefficient
ρ	density, kg m^{-3}
σ	surface tension, N m^{-1}
Φ_i	Poynting factor
$\Phi_{v,0}/W$	space velocity, Nm^3 kg_{cat}^{-1} s^{-1}

Sub- and Superscripts

B	large bubbles	*large*	refering to large bubbles
c	coolant	*out*	outlet conditions
DF	dense phase	*P*	catalyst phase
G	gas phase	*R*	reactor
i	component	*ref*	reference conditions
in	inlet conditions	*S*	slurry phase
j	reaction	*small*	refering to small bubbles
L	liquid phase		

Kinetic and selectivity parameters (see List of Symbols for Chapters 2-6):
$a, b, k, K_P, k_{WGS}, K, t_P^1, t_P^2, k_R^2, p, t_O, k_R, c, \alpha_n, \theta_n$

References

[1] Saxena, S.C.; Rosen, M.; Smith, D.N.; Ruether, J.A., Mathematical modeling of Fischer-Tropsch slurry bubble column reactors, *Chem. Eng. Commun.* **1986**, *40*, 97–151.

[2] Saxena, S.C., Bubble column reactors and Fischer-Tropsch synthesis, *Catal. Rev.-Sci. Eng.* **1995**, *37*, 227–309.

[3] Calderbank, P.H.; Evans, F.; Farley, R.; Jepson, G.; Poll, A., Rate processes in the catalyst-slurry Fischer-Tropsch reaction, *Catal. in Practice* **1963**, 66–74.

[4] Satterfield, C.N.; Huff, G.A., Effects of mass transfer on Fischer-Tropsch synthesis in slurry reactors, *Chem. Eng. Sci.* **1980**, *35*, 195–202.

[5] Deckwer, W.-D.; Serpemen, Y.; Ralek, M.; Schmidt, B., On the relevance of mass transfer limitations in the Fischer-Tropsch slurry process, *Chem. Eng. Sci.* **1981**, *36*, 765–771.

[6] Deckwer, W.-D.; Serpeman, Y.; Ralek, M.; Schmidt, B., Modeling the Fischer-Tropsch synthesis in the slurry phase, *Ind. Eng. Chem. Process Des. Dev.* **1982**, *21*, 231–241.

[7] Bukur, D.B., Some comments on models for Fischer-Tropsch reaction in slurry bubble column reactors, *Chem. Eng. Sci.* **1983**, *38*, 441–446.

[8] Stern, D.; Bell, A.T.; Heinemann, H., Effects of mass transfer on the performance of slurry reactors used for Fischer-Tropsch synthesis, *Chem. Eng. Sci.* **1983**, *38*, 597–605.

[9] Kuo, J.C.W., Slurry Fischer-Tropsch/Mobil two stage process of converting syngas to high octane gasoline, Final report DOE-PC-3022-10, DOE **1983**.

[10] Stenger, H.G.; Satterfield, C.N., Effects of sulfur poisoning of a reduced fused magnetite catalyst in the Fischer-Tropsch synthesis, *Ind. Eng. Chem. Process Des. Dev.* **1985**, *24*, 415–420.

[11] Prakash, A.; Bendale, P.G., Design of slurry reactor for indirect liquefaction applications, Final report DE-AC22-89PC89870, DOE **1991**.

[12] Prakash, A., On the effects of syngas composition and water-gas-shift reaction rate on FT synthesis over iron based catalyst in a slurry reactor, *Chem. Eng. Commun.* **1994**, *1280*, 143–158.

[13] De Swart, J.W.A., *Scale-up of a Fischer-Tropsch reactor*, Ph.D. thesis, University of Amsterdam, Amsterdam, The Netherlands **1996**.

[14] Mills, P.L.; Turner, J.R.; Ramachandran, P.A.; Dudukovic, M.P., The Fischer-Tropsch synthesis in slurry bubble column reactors: analysis of reactor perfor-

mance using the axial dispersion model, in K.D.P. Nigam; A. Schumpe, eds., *Three-phase sparged reactors*, Gordon & Breach, Amsterdam, 1996 pp. 339–386.

[15] Inga, J.R.; Morsi, B.I., A novel approach for the assessment of the rate-limiting step in Fischer-Tropsch slurry process, *Energy Fuels* **1996**, *10*, 566–572.

[16] Krishna, R.; Maretto, C., Scale up of a bubble column slurry reactor for Fischer-Tropsch synthesis, *Stud. Surf. Sci. Catal.* **1998**, *119*, 197–202.

[17] De Swart, J.W.A.; Krishna, R.; Sie, S.T., Selection, design and scale up of the Fischer-Tropsch reactor, *Stud. Surf. Sci. Catal.* **1997**, *107*, 213–218.

[18] Graaf, G.H.; Sijtsema, P.J.J.M.; Stamhuis, E.J.; Joosten, G.E.H., Chemical equilibria in methanol synthesis, *Chem. Eng. Sci.* **1986**, *41*, 2883–2890.

[19] Deckwer, W.-D.; Louisi, Y.; Zaidi, A.; Ralek, M., Hydrodynamic properties of the Fischer-Tropsch slurry process, *Ind. Eng. Chem. Process Des. Dev.* **1980**, *19*, 699–708.

[20] Krishna, R.; De Swart, J.W.A.; Ellenberger, J.; Martina, G.B.; Maretto, C., Gas holdup in slurry bubble columns: effect of column diameter and slurry concentrations, *AIChE J.* **1997**, *43*, 311–316.

[21] Krishna, R.; Ellenberger, J., Gas holdup in bubble colum reactors operating in the churn-turbulent regime, *AIChE J.* **1996**, *42*, 2627–2634.

[22] Letzel, M.H.; Schouten, J.C.; Krishna, R.; Van den Bleek, C.M., Gas holdup and mass transfer in bubble column reactors operated at elevated pressure, *Chem. Eng. Sci.* **1999**, in press.

[23] Vermeer, D.J.; Krishna, R., Hydrodynamics and mass transfer in bubble columns operating in the churn-turbulent regime, *Ind. Eng. Chem. Process Des. Dev.* **1981**, *20*, 475–482.

[24] Lox, E.S.; Marin, G.B.; de Graeve, E.; Bussiere, P., Characterization of a promoted precipitated iron catalyst for Fischer-Tropsch synthesis, *Appl. Catal. A* **1988**, *40*, 197–218.

[25] Tareef, M., *Colloid J. USSR* **1940**, *6*, 545, cited in *Ind. Eng. Chem. Process Des. Dev.* **1980**, *19*, 699–708.

[26] Marano, J.J.; Holder, G.D., General equation for correlating the thermophysical properties of n-paraffins, n-olefins, and other homologous series. 2.Asymptotic behavior correlations for PVT properties, *Ind. Eng. Chem. Res.* **1997**, *36*, 1895–1907.

[27] Marano, J.J.; Holder, G.D., General equation for correlating the thermophysical properties of n-paraffins, n-olefins, and other homologous series. 3.Asymptotic

behavior correlations for thermal and transport properties, *Ind. Eng. Chem. Res.* **1997**, *36*, 2399–2408.

[28] Marano, J.J.; Holder, G.D., Characterization of Fischer-Tropsch liquids for vapor-liquid equilibria calculations, *Fluid Phase Equilib.* **1997**, *138*, 1–21.

[29] Erkey, C.; Rodden, J.B.; Akgerman, A., A correlation for predicting diffusion coefficients in alkanes, *Can. J. Chem. Eng.* **1990**, *68*, 661–665.